

DCPR-GAN: Dental Crown Prosthesis Restoration Using Two-Stage Generative Adversarial Networks

Sukun Tian^{ID}, Miao Hui Wang^{ID}, Member, IEEE, Ning Dai, Member, IEEE, Haifeng Ma^{ID}, Member, IEEE, Linlin Li, Luca Fiorenza, Yuchun Sun^{ID}, and Yangmin Li^{ID}, Senior Member, IEEE

Abstract—Restoring the correct masticatory function of broken teeth is the basis of dental crown prosthesis rehabilitation. However, it is a challenging task primarily due to the complex and personalized morphology of the occlusal surface. In this article, we address this problem by designing a new two-stage generative adversarial network (GAN) to reconstruct a dental crown surface in the data-driven perspective. Specifically, in the first stage, a conditional GAN (CGAN) is designed to learn the inherent relationship between the defective tooth and the target crown, which can solve the problem of the occlusal relationship restoration. In the second stage, an improved CGAN is further devised by considering an occlusal groove parsing network (GroNet) and an occlusal fingerprint constraint to enforce the generator to enrich the functional characteristics of the occlusal surface. Experimental results demonstrate that the proposed framework significantly outperforms the state-of-the-art deep learning

Manuscript received February 5, 2021; revised April 30, 2021 and June 21, 2021; accepted October 6, 2021. Date of publication October 12, 2021; date of current version January 5, 2022. This work was supported in part by the National Natural Science Foundation of China under Grant 52105265, in part by the National Key R&D Program of China under Grant 2019YFB1706900, in part by the Natural Science Foundation of Shenzhen City under Grant 20200805200145001, in part by the Open Fund of Hubei Key Laboratory of Mechanical Transmission and Manufacturing Engineering, Wuhan University of Science and Technology under Grant MTMEOF2020B06, and in part by the Beijing Training Project for the Leading Talents in S&T under Grant Z191100006119022. (Sukun Tian and Miao Hui Wang contributed equally to this work.) (Corresponding authors: Haifeng Ma, Yuchun Sun, and Ning Dai)

Sukun Tian and Haifeng Ma are with the Key Laboratory of High Efficiency and Clean Mechanical Manufacture Ministry of Education, School of Mechanical Engineering, Shandong University, Jinan 250061, China (e-mail: sukhum169@sdu.edu.cn; mahaifeng@sdu.edu.cn).

Miao Hui Wang is with the School of Computer Science and Technology, Hainan University, Haikou 570228, China, and also with Guangdong Key Laboratory of Intelligent Information Processing, Shenzhen University, Shenzhen 518060, China (e-mail: wang.miaohui@gmail.com).

Ning Dai is with the College of Mechanical and Electrical Engineering, Nanjing University of Aeronautics and Astronautics, Nanjing 210016, China (e-mail: daining@nuaa.edu.cn).

Linlin Li and Yuchun Sun are with the Department of Prosthodontics, School and Hospital of Stomatology, Peking University, Beijing 100081, China (e-mail: sdlli0511@163.com; kqsyc@bjmu.edu.cn).

Luca Fiorenza is with the Department of Anatomy and Developmental Biology, Monash University, Melbourne VIC 3800, Australia (e-mail: luca.fiorenza@monash.edu).

Yangmin Li is with the Department of Industrial and Systems Engineering, Hong Kong Polytechnic University, Hong Kong (e-mail: yangmin.li@polyu.edu.hk).

Digital Object Identifier 10.1109/JBHI.2021.3119394

methods in functional occlusal surface reconstruction using a real-world patient database. Moreover, the standard deviation (SD) and root mean square (RMS) between the generated occlusal surface and the target crown calculated by our method are both less than 0.161 mm. Importantly, the designed dental crown have enough anatomical morphology and higher clinical applicability.

Index Terms—Dental crown restoration, generative adversarial networks, occlusal fingerprint, occlusal surface.

I. INTRODUCTION

DENTAL caries, as a common chronic oral disease, can cause a series of complications such as dental pulp disease and oral maxillofacial inflammation [1]–[3]. The *Global Burden of Disease Study 2016* [4] reported that at least 3.58 billion people worldwide are affected by oral pathologies, and approximately 67.04% of adults over 20-years-old suffer from *dental caries*, which is the leading cause of tooth defects [5], [6]. In the clinical practice of dentistry, it is really challenging to rebuild teeth with morphological diversity encompassed by tooth morphology and their specific occlusal fingerprints (see Fig. 1). Consequently, *computer-aided geometric design* (CAGD) has been employed to improve the efficiency of the *dental crown prosthesis* (DCP) restoration.

Most CAGD-based DCP restoration systems, such as *3Shape*, *Duret* and *OrthoCAD*, take the standard tooth template library as an important part of the oral prosthetic software [7]–[9]. Although the combination of CAGD and prosthetic dentistry leads to many advantages, the maxillofacial morphology quality of DCP depends on the proficiency of the dental practitioner. For instance, bionic-based DCP design requires many tooth samples and manual interactions. It requires decisions like what the most suitable occlusal surface is, how many feature points should be selected, and how to quantify the occlusal functional area for 32 categories of tooth. Therefore, it is urgent to develop a data-driven DCP restoration to relieve the workload of dentists as well as to reduce the cost of dental restoration.

As far as we know, the massive DCP point cloud data obtained by prosthodontics has not been explored as a means to develop a data-based DCP restoration that improves the restoration quality and efficiency. Thus, we believe that developing a new *deep*

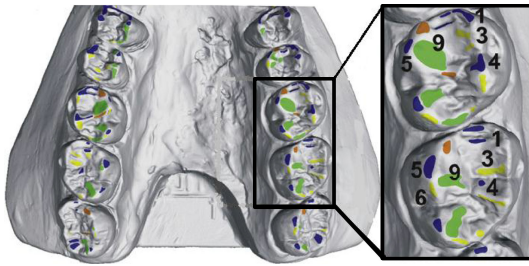


Fig. 1. Schematic illustration of the occlusal fingerprint distribution of the maxillary molars [10]. Here, regions 1, 4, and 5 are in contact during laterotrusive; regions 3 and 6 denote lateroprotrusive; region 9 denotes medioltrusive.

learning (DL)-driven DCP restoration method is a promising way to move dental caries technology from digital platforms to intelligent designs. However, developing a DL-based DCP framework is challenging: 1) There is no large enough tooth defect database to train a restoration deep neural network (DNN); 2) The size and shape of defective teeth vary dramatically among subjects, raising difficulties in DNN model training; 3) A suitable occlusal contact relationship between the generated occlusal surface and its opposite tooth is difficult to develop.

Recently, some early DL-aided occlusal surface designs [11]–[13] have been developed for dental-related diseases, but not for DCP. Among these accomplishments, DL-based approaches have been proposed for dental diagnosis, tooth segmentation and dental restorations. Hatvani *et al.* [14] adopted a subpixel convolutional neural network (CNN) and a U-net to improve the resolution of 2-D cone-beam computed tomography (CBCT) image slices of *ex vivo* teeth. Zhang *et al.* [15] extracted the tooth preparation margin line with a 3D CNN which is based on a sparse octree (S-Octree) structure. Lian *et al.* [16] designed an end-to-end DNN network (called MeshSegNet) to automatically label the individual tooth on a raw dental surface. However, it should be noted that because most of these methods are designed for some specific dental tasks other than DCP restoration, they are limited to the reconstruction of functional occlusal surface. Meanwhile, the successful application of the above methods indicates that deep learning has great application potential in the field of dental crown prosthesis restoration. Recently, a few previous studies have adopted generative model for occlusal surface reconstruction, through which the relationship among missing teeth and target data can be captured. For example, Hwang *et al.* [17] applied a DNN network based on the Pix2pix [18] model to design synthetic dental crowns. Similar to [17], Yuan *et al.* [19] developed a Pix2pix-based network for occlusal surface generation by combining the perceptual adversarial loss. However, the above methods do not consider the influence of dental biological morphology (occlusal fingerprint, occlusal groove) on the reconstruction of the occlusal surface, so that the occlusal surface generated by these methods does not have the anatomical morphology of natural teeth.

In this article, a new dental crown prosthesis restoration using a two-stage deep generative adversarial network (denoted as “DCPR-GAN”) is developed to address the problem in reconstructing the functional occlusal surface for a defective tooth.

The key factor to evaluate the success of restoration treatment is to ensure that the designed dental crown prosthesis has the correct occlusal contact relationship and sufficient natural tooth anatomical morphological characteristics. In view of this, an occlusal surface design pattern based on hierarchical representation of functional features is adopted to reconstruct the overall organizational structure and functional features of the occlusal surfaces in turn. Different from the previously mentioned DL-based methods, the proposed method has several benefits: 1) It is suitable for the restoration of different categories of teeth; 2) It avoids the problem that the traditional restoration method is difficult to adapt to the patient’s dentition; 3) It is highly efficient to design a crown prosthesis that is an accurate representation of the occlusal surface. Specifically, the main contributions of this approach are:

- 1) We established a large scale 3D dental crown database provided by professional hospitals. To the best of our knowledge, it is the first public database for DL-based model training in dental crown prosthesis restoration.
- 2) To solve the challenging problem of functional feature generation, we divide the restoration task into two stages: the first stage (Stage-I) generates the global structure by considering the spatial constraints on the occlusal surface. The second stage (Stage-II) takes the occlusal fingerprint and the Stage-I result as the input and synthesizes functional occlusal surface with realistic details of the dental crown.
- 3) We design a generative adversarial network (GAN)-driven DCP restoration framework for generating dental crown prosthesis, including dental depth generation, two-stage deep networks, and prosthesis design. The proposed DCPR-GAN scheme demonstrates superior performance on a real-world dental database with sufficient anatomical morphology to have high clinical applicability.

The remainder of this article is organized as follows. We present the detailed methodology in Section II. The database, experimental results, and the comparison results between state-of-the-art methods are described in Section III. Finally, conclusion and discussion are summarized in Section IV.

II. METHODS

A flowchart of the proposed DCPR-GAN framework is illustrated in Fig. 2. An orthographic projection method is first designed to generate the dental depth maps. In the dental crown restoration step, robust deep adversarial networks are designed to reconstruct a dental crown image, in which a two-stage GAN is developed to improve the quality of generated dental occlusal surface. Specifically, the task of the first-stage GAN model (Stage-I GAN) is to describe the inherent associations between defective teeth and their tissue structures with the corresponding target data. The task of the second-stage GAN model (Stage-II GAN) is to reconstruct the fine-grained tissue structure by considering the occlusal fingerprint distribution and occlusal groove. In the DCP design step, several objective metrics are performed to guarantee the generated occlusal surface quality. Finally, a dental prosthesis with a functional occlusal surface is created consistent with the proposed framework.

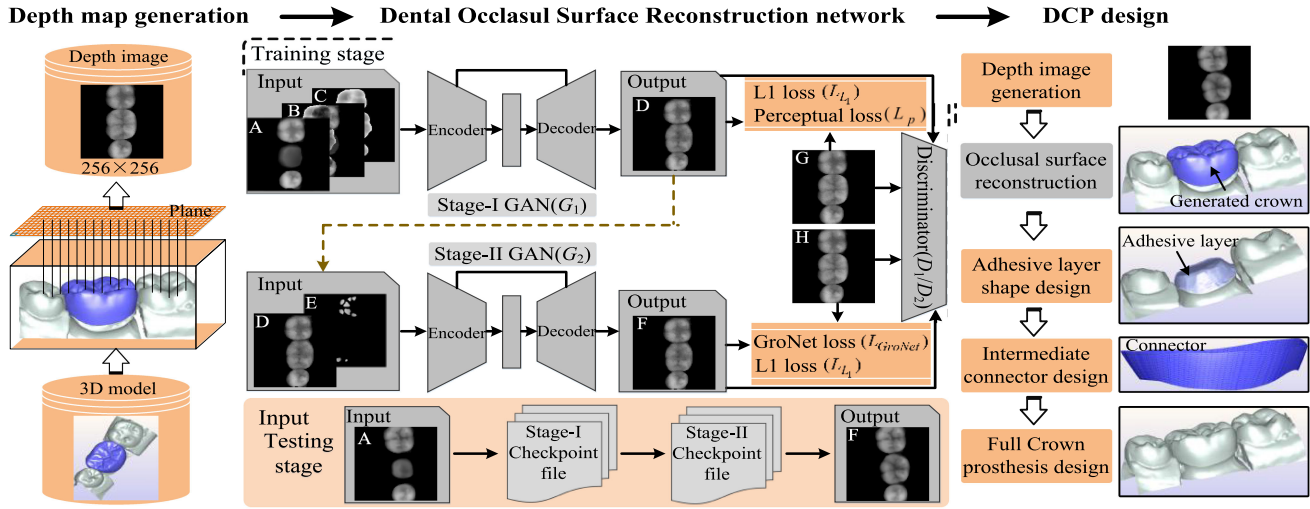


Fig. 2. Overview of the proposed DCPR-GAN for dental crown prosthesis restoration: A-Preparation, B-Gap distance, C-Opposing jaw, D-Initial occlusal surface, E-occlusal fingerprint, F-The functional occlusal surface, G-Target crown without the occlusal fingerprint, and H-Target crown with the occlusal fingerprint.

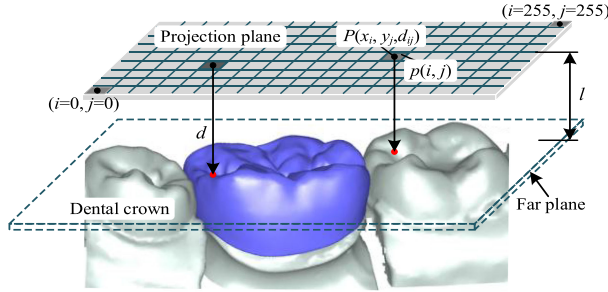


Fig. 3. Illustration of the depth map generation.

A. Depth Map Generation

Before extracting dental features, tooth morphology is represented as a depth map that contains all the spatial information for training a deep model. In the case of occlusal surface morphology generation, the depth maps capture the surface detail feature in a compact way. To improve retrieval efficiency and accuracy, the bounding box and virtual rotating sphere technology are adopted to normalize the preprocessing of the 3D dental model data so that similar models with different coordinate systems have the same similarity. In addition, an adaptive visual distance-based orthogonal projection is designed to fully preserve the spatial shape information. Specifically, the projection plane is adaptively adjusted to the bounding box of the dental model in the direction of the determined viewing angle so that the projected dental crown image is richer and more distinguishable.

The dental depth map is obtained by considering the distance of the crown surface to a projection plane as shown in Fig. 3. The projection plane is located at a proper distance parallel to the bounding box of the dental model, which is divided into 256×256 grids. Then, the shortest distance d_{ij} at the position (i, j) on the projection plane to the dental crown surface is calculated. In addition, a far plane from the projection plane l is defined,

and the coordinate origin is set at the lower left corner of the far plane. It is stipulated that the dental crown model beyond this plane will not be projected but it will be converted into a pixel value of 0 in the depth map. Finally, the shortest vertical distance d from the center point of each grid to the occlusal surface is considered and converted into the depth magnitude value $p(i, j)$ that is formulated as:

$$p(i, j) = \begin{cases} Max_I, & d = 0 \\ 255 - Max_I \times d^n / l^n, & 0 < d < l \\ 0, & d \geq l \end{cases}, \quad (1)$$

where Max_I denotes the maximum magnitude value (e.g., 255 for 8-bits), n is an image enhancement factor, and l denotes the distance threshold. Based on a large number of experiments, the functional characteristic information of an occlusal surface can be retained when $n = 2$ and $l = 6$ mm.

B. Two-Stage Dental Crown Restoration Network

In this step, GAN is leveraged to refine the generator to produce an occlusal surface that satisfies the correct masticatory function. This is accomplished by designing a two-stage GAN architecture to reconstruct the occlusal surface. As it is very challenging to generate a functional occlusal surface directly based on the occlusal fingerprint and groove characteristics, a two-stage gradual adjustment strategy is employed with each stage focusing on one specific target (Fig. 2). At Stage-I, the basic shape of an occlusal surface that satisfies the spatial positional relationship is produced and at Stage-II the details of the occlusal surface are completed by adding an occlusal groove parsing network (GroNet) loss and an occlusal fingerprint constraint. GroNet is pre-trained by the Stage-I GAN model and its parameters. After the network converges, it is remained fixed and loaded into the Stage-II network as a constraint to further enhance the harmony of the generated occlusal groove and the object groove pixels. Fig. 4 illustrates the proposed

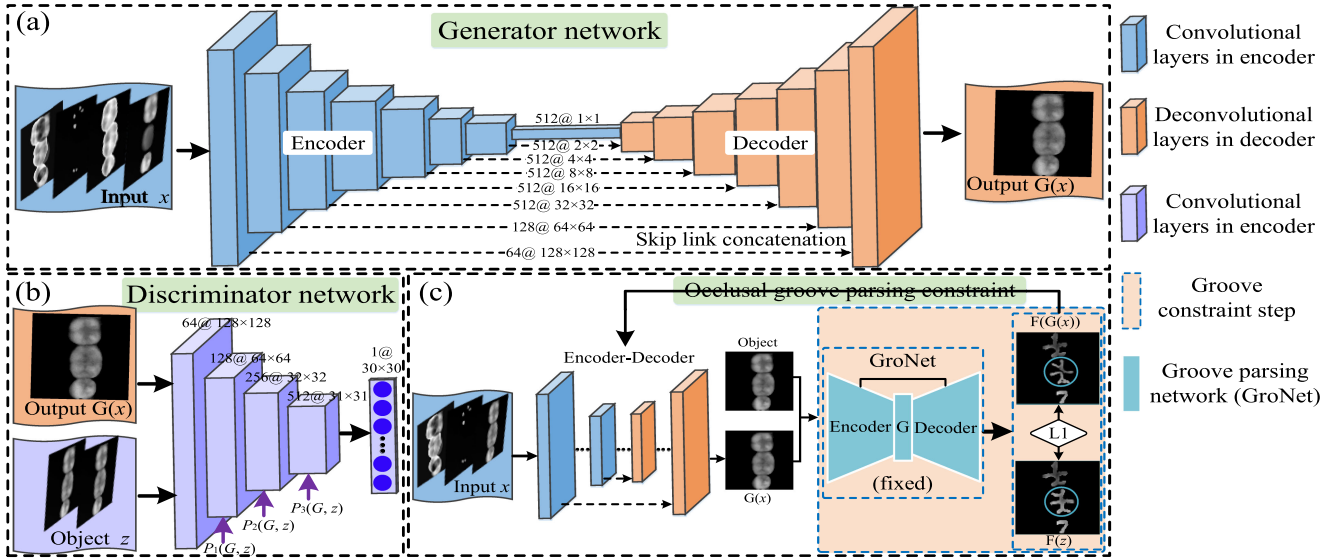


Fig. 4. Network architectures of the proposed two-stage DCPR-GAN: (a) Generator network, (b) Discriminator network, (c) Occlusal groove parsing network. Stage-I GAN consists of (a) and (b), while Stage-II GAN consists of (a), (b) and (c). The generator network is composed of some blocks of Convolution-BatchNorm-ReLU encoding layers and Deconvolution-BatchNorm-ReLU decoding layers, where the skip-connections are used between the mirrored layers. The discriminator network consists of Convolution-BatchNorm-LReLU layers, where P_1 , P_2 and P_3 layers are utilized to evaluate the perceptual adversarial loss. The occlusal groove parsing network (GroNet) is a pre-trained network, which is to further ensure the realistic performance of the generated occlusal surface.

DCPR-GAN architecture that is composed of two generative adversarial networks.

1) Initial Occlusal Surface Generation (Stage-I GAN): Inspired by the two-player zero-sum game, GAN is composed of a generator G and a discriminator D , both of which are trained with the adversarial learning mechanism [20], [21]. The aim of GAN is to model the potential distribution of existing data and generate a new data sample with the same distribution. In this article, an additional conditioning variable c is employed into the traditional GAN with the following objective function $V(D, G)$,

$$\begin{aligned} \min_G \max_D V(D, G) = & \mathbb{E}_{x \sim P_{data(x)}} [\log D(x|c)] \\ & + \mathbb{E}_{z \sim P_{z(z)}} [\log (1 - D(G(z|c)))] , \end{aligned} \quad (2)$$

where $\mathbb{E}(\cdot)$ denotes the expectation operator, x is the real image sampled from the real data distribution $P_{data(x)}$, and z denotes an input sample from a prior distribution $P_{z(z)}$. The generator G takes some noisy samples z as inputs, learns a complex mapping relationships over real training samples x , and tries to map the distribution $P_{z(z)}$ to the real data distribution $P_{data(x)}$. Meanwhile, the discriminator D is used as a binary classifier to distinguish the generated image $G(z|c)$ and real image x . In other words, the generator G aims to minimize the distribution distance between $G(z|c)$ and x , while the goal of the discriminator D is to maximize the distribution between them.

Instead of directly generating a functional surface conditioned on the occlusal fingerprint distribution, the strategy here is to generate a basic morphology with at the first stage that focuses on the occlusion spatial relationship. The adversarial loss encourages the distribution of the generated data sample to be very similar to the actual morphology. However, the standard GAN

loss does not directly penalize the instance-to-instance mapping. Therefore, we design a new comprehensive generation loss L_{G_1} for the first stage by adopting the generative loss $L_{Stage-I}$, L_1 distance loss $L_{L1}(G_1)$ and a perceptual generation loss $L_p(G_1)$.

$$\begin{aligned} L_{G_1} = & \arg \min_{G_1} L_{Stage-I}(G_1, D_1) \\ & + \lambda_{L1} L_{L1}(G_1) + \lambda_{pG} L_p(G_1), \end{aligned} \quad (3)$$

where the first term is the generative loss, λ_{L1} and λ_{pG} are the balance weights of the corresponding loss functions.

The improved adversarial loss L_{D_1} is composed of the standard adversarial loss and a perceptual adversarial loss $L_{p(D_1)}$,

$$L_{D_1} = \arg \max_{D_1} L_{Stage-I}(G_1, D_1) + \lambda_{pD} L_p(D_1). \quad (4)$$

where the first term is the adversarial loss, and λ_{pD} is a balance weight factor.

In clinical practice, the full functionality of the defective teeth cannot be restored by focusing only on the anatomical features of the occlusal surface and its spatial position. Furthermore, the contact between the upper and lower teeth during masticatory movement must be considered. That is, the ideal prosthetic occlusal surface has a certain amount of interference intensity with its opposing teeth [22]. Here, the preparation tooth x_1 , the opposing tooth c_1 , the tooth type label \hat{c} , target crown without the occlusal fingerprint z_1 are used, and gap distance d between two jaws as the constraints to measure the occlusal spatial relationship, which guides the generator G_1 to produce a crown surface with the correct occlusal relationship. The conditional

adversarial loss is reformulated as,

$$\begin{aligned} L_{Stage-I}(G_1, D_1) = & \mathbb{E}_{x_1, c_1, d, z_1, \hat{c}} [\log D_1(x_1, c_1, d, z_1, \hat{c})] \\ & + \mathbb{E}_{x_1, c_1, d, \hat{c}} [\log (1 - D_1(G_1(x_1, c_1, d, \hat{c}), x_1, c_1, d, \hat{c}))]. \end{aligned} \quad (5)$$

To further improve the ability to reconstruct anatomical features, the perceptual loss is introduced into the DCPR-GAN model. The high-dimensional feature deviation between the generated occlusal surface and the target crown in the hidden layers of the discriminator D_1 are measured. Through an adversarial process, the discriminator D_1 is able to maximally capture the discrepancy between them. Conversely, the generator G_1 tries to enforce the generated occlusal surface close to the target crown. The perceptual generation loss function is then formulated as,

$$L_p(G_1) = \mathbb{E}_{x_1, c_1, z_1} \left[\sum_i \lambda_i \frac{1}{C_i H_i W_i} \sum_{i=1}^N \|h_i(z_1) - h_i(G_1)\| \right], \quad (6)$$

where λ_i is a balance weight factor, and $C_i \times H_i \times W_i$ is the shape of the i -th hidden layer h_i .

Finally, the perceptual adversarial loss is,

$$L_p(D_1) = \mathbb{E}_{x_1, c_1, z_1} [\max \{0, m - L_p(G_1)\}]. \quad (7)$$

where m is a positive margin value.

2) Functional Occlusal Surface Generation (Stage-II GAN):

DCP restoration faces a complex oral environment. The occlusal relationship determines the contact form, position and the range between teeth, which has an important impact on the occurrence and distribution of the occlusal fingerprint. The occlusal fingerprint analysis method describes the jaw movements of an individual by examining the structural parameters. Because the occlusal fingerprint reflects the individual occlusal relationship and masticatory behavior, it can be used for individual identification and fingerprint recognition [23]. The Physiological wear on the teeth makes the maxillofacial contact between upper and lower teeth variable, which helps to eliminate some early occlusive contact points, and reduces the lateral force and occlusal balance.

The generator G_1 in the first stage produces a coarse occlusal surface but one that is similar to the target crown in pose and basic shape. We hence perform the generator G_2 at the second stage to generate fine-grained occlusal surface features that enforces the initial crown closer to the target. As shown in Fig. 2, the Stage-II GAN takes the first stage results x_2 and the occlusal fingerprint as input and enriches the functional characteristics. The new generation loss L_{G2} is defined as,

$$\begin{aligned} L_{G2} = & \arg \min_{G_2} L_{Stage-II}(G_2, D_2) + \lambda_{L1} L_{L1}(G_2) \\ & + \lambda_{GroNet} L_{GroNet}, \end{aligned} \quad (8)$$

where the first term is the generative loss, $L_{L1}(G_1)$ is $L1$ distance loss, L_{GroNet} denotes the GroNet loss, and λ_{L1} and λ_{GroNet} are the balance weights of the corresponding loss functions, respectively.

Finally, the adversarial loss is,

$$L_{D2} = \arg \max_{D_2} L_{Stage-II}(G_2, D_2). \quad (9)$$

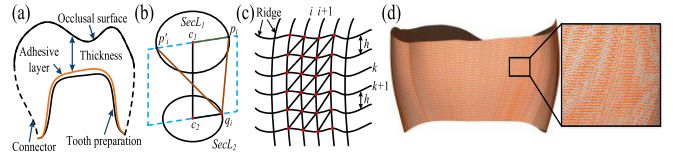


Fig. 5. Illustrations of dental crown design workflow. (a) The Sketch map of the adhesive layer and connector design, (b) The schematic diagram of the plane intersection method, (c) Mesh generation, (d) The designed connector.

In the second stage, the occlusal fingerprint c_2 is adopted as a constraint to measure the functional features, which can guide the generator G_2 to produce an occlusal surface that satisfies the correct masticatory function. To compute the generation $G(x_2)$ with the target crown with the occlusal fingerprint z_2 , we also adopt the $L1$ distance as the generation loss of the second stage, and then the conditional adversarial loss is reformulated by,

$$\begin{aligned} L_{Stage-II}(G_2, D_2) = & \mathbb{E}_{x_2, c_2, z_2} [\log D_2(x_2, c_2, z_2)] \\ & + \mathbb{E}_{x_2, c_2, \hat{c}} [\log (1 - D_2(G_2(x_2, c_2, \hat{c}), c_2, \hat{c}))]. \end{aligned} \quad (10)$$

The complex tooth crown morphology determines the direction of food flow and masticatory efficiency during the chewing process. Therefore, restoring a correct groove shape is also an important factor to evaluate the success of the DCP restoration. With the goal of reconstructing the fine-grained tissue structure of the occlusal surface, a new GroNet is introduced to further ensure the generated surface with more crown-realistic features. In the parsing network, the discrepancy between both the occlusal grooves is minimized by an $L1$ regularization, and the proposed groove loss is defined as,

$$L_{GroNet} = \mathbb{E}_{x, c, z} [\|F(z) - F(x, c)\|_1], \quad (11)$$

where $\|\cdot\|$ represents the $L1$ norm, z is a target tooth, c is the opposite occlusal tooth, x denotes a noise image, and $F(\cdot)$ denotes an occlusal network that is used to extract the occlusal groove of a generated surface and its corresponding target crown.

C. Light-Weight Intermediate Connector Design

Before the design process, the first step is to offset the upper part of the tooth preparation by a given distance to simulate the use of an adhesive layer (see Fig. 5(a)). The second step is to design the connector mesh surface by using the boundary curves of the generated occlusal surface ($SecL_1$) and the adhesive layer ($SecL_2$) as the reference lines. To improve the shape control over the connector surface, a skinning operation based on the B-spline interpolation is used to automatically design the intermediate connector, where the skinning is a common method of surface definition in the CAD system [8].

The connector is designed according to the following five steps: (1) Extracting all points of the boundary curve $SecL_2$, which is $SecQ = \{q_i | i = 1, 2, \dots, n\}$; (2) Using $SecQ$ as the reference point sequence, and adopting “plane intersection method” to calculate the corresponding matching point sequence $SecP$ on the boundary curve $SecL_1$, that is $SecP = \{p_i | i = 1, 2, \dots, n\}$. The schematic diagram is shown in Fig. 5(b), where the intersection points on $SecL_1$ are calculated by using the plane

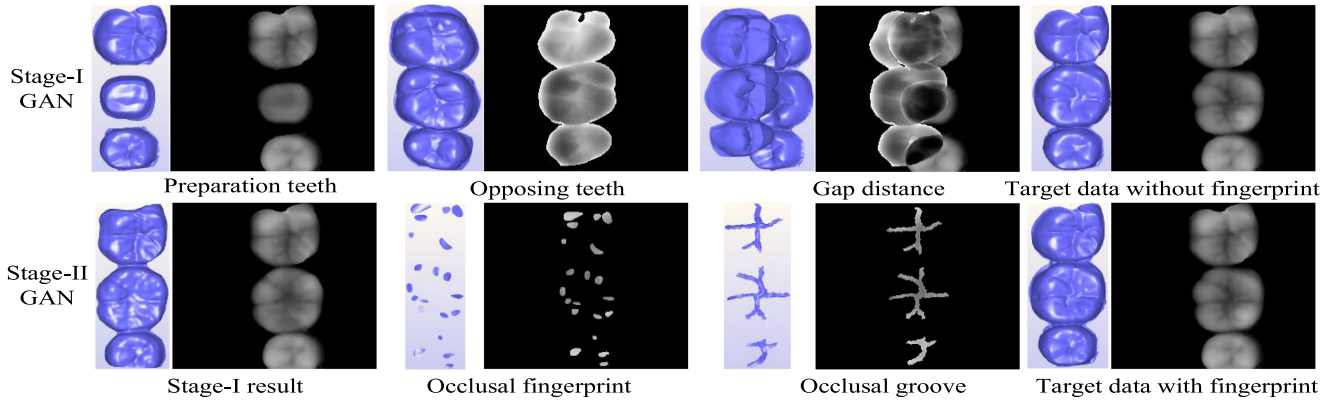


Fig. 6. Illustrations of tooth samples for various stages.

TABLE I
DETAIL INFORMATION ABOUT OUR DENTAL CROWN DATABASE

Type	Different age groups			Total
	35-40	41-45	46-50	
#36	157	132	99	388
#46	141	118	133	392

constructed by two centers (c_1, c_2) and a reference point q_i . As the boundary curve is closed, two points (p_i and p'_i) intersect, if $\angle p_i q_i c_2 > \angle p'_i q_i c_2$, then p_i is the corresponding matching point to q_i , and otherwise p'_i is the estimated intersection point; (3) Calculating the midpoint sequence $SecK$ of two sets for the reference point sequences: $k_i = (p_i + q_i)/2$, $i = 1, 2, \dots, n$; (4) Taking (p_i, k_i, q_i) as a set of control points, the B-spline curve is used to obtain the ridge and then is uniformly discretized (see Fig. 5(c)); (5) Connecting the intersection points between two adjacent ridges sequentially to obtain the triangular mesh surface (see Fig. 5(d)).

III. EXPERIMENTS AND RESULTS

A. Dental Dataset Preparation

To our knowledge, there is no public dental crown prosthesis database to support learning-based methods for training. Therefore, a dental crown database is built first to facilitate DL-based studies in the community. As we do not have enough manpower or professional knowledge of stomatology to collect the damaged and repaired teeth of patients, it is difficult to collect a sufficient number of dental samples for the deep network training. Therefore, this project involves a collaboration with *Peking University Hospital of Stomatology* and *Nanjing Stomatological Hospital*, where some dentists provide the manually extracted occlusal fingerprints. The 3D digital dental database is collected using the dental scanner (D700, 3Shape, Denmark), and the total number of dental samples is 780. Detailed information on the database is summarized in Table I. Every sample contains an occlusal groove, an occlusal fingerprint, a preparation tooth, an opposing tooth, a target crown without the occlusal fingerprint and a target crown with the occlusal fingerprint (Fig. 6).

TABLE II
PARAMETER VALUES OF THE PROPOSED NETWORK

Parameter	Value	Parameter	Value
L_1 loss λ_{L_1}	100	Groove loss λ_{GroNet}	50
$L_p(D)$ loss λ_{pD}	100	Learning rate	0.00002
$L_p(G)$ loss λ_{pG}	50	Momentum β_1	0.5
$P_1(G, x)$ weight λ_1	1	Momentum β_2	0.999
$P_2(G, x)$ weight λ_2	2	ReLU slope	0.2
$P_3(G, x)$ weight λ_3	2	m	0.35

Many studies have reported that the highest rate of dental caries is on the mandibular first molar [24], [8], [22], so patients with the defective teeth #36 or #46 are selected as the main research objects. The code implementation and database related to this paper can be downloaded at <https://github.com/Sukhum169>.

B. Training Details

For the two-stage generative network training, the dental samples are randomly divided into two parts: 700 (355 #36, and 345 #46) for training, and the remaining 80 samples for testing. The proposed DCPR-GAN networks are implemented on the *Tensorflow* framework [25], and all experiments are performed on a personal computer (PC) with an *Intel (R) Platinum 8168 CPU @ 2.70 GHz* with 128GB RAM and a *GeForce GTX 1080Ti GPU*. To train the two-stage GANs, the networks are optimized using the *Adam* solver with the parameters shown in Table II.

Fig. 7 plots the training loss of DCPR-GAN over iteration, and demonstrates that the loss value decreases consistently as training progresses. The DCPR-GAN achieves a steady decrease of loss value, indicating that the generative model can learn the sample features and deliver a desirable occlusal surface of the defective tooth.

C. Effectiveness of Two-Stage Generator Network

Stage-I GAN is trained to verify the effectiveness of the occlusal fingerprint as guiding condition. As shown in Fig. 8, the distributions of the generated dental patterns (see Fingerprint-Output) are very close to the target position (see

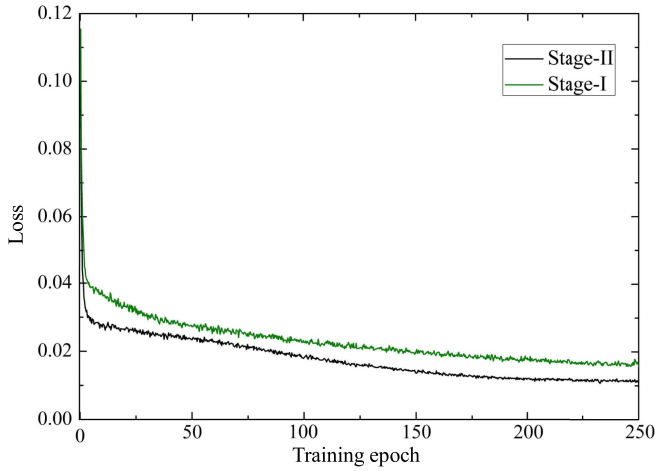


Fig. 7. Training curves of Stage-I and Stage-II.

Fingerprint-Object). Stage-I GAN synthesizes a reasonable occlusal surface (see Crown-Stage-I) that captures the global structure of a crown, such as dental cusps and grooves. However, the first-stage results are coarse with various missing details.

The occlusal surface generated by the Stage-II GAN is more realistic (see Crown-Stage-II), and the distribution of the dental cusp-fossa is more pronounced. This demonstrates that the occlusal surface generated by the Stage-II GAN better reflects the functional characteristics of the teeth.

Finally, to further verify the performance of our DCPR-GAN and analyze the influence of the occlusal groove shape constraint on the generator, the occlusal grooves of the first (see Groove-Stage-I) and second (see Groove-Stage-II) stage results are extracted by using GroNet. The Groove-Stage-II is very similar to the Groove-Object as shown in Fig. 8. This indicates that the GroNet loss plays an expected role in crown restoration and has a positive impact on the shape of the generated crown.

D. Comparison Results with State-of-the-Art Methods

1) Quantitative Results: Using the test data introduced in Section III-A, the DCPR-GAN is compared with five state-of-the-art approaches, including Pix2pix [18], Pix2pixHD [26], perceptual adversarial network (PAN) [21], generative face completion (GFC) network [27], and dental occlusal surface generator network (Dental-GAN) [19]. Additionally, the proposed method is compared with a variant of Stage-I GAN, where the GroNet loss and the occlusal fingerprint constraint are added to the Stage-I GAN (denoted as Stage-I GroNet_OF).

Pix2pix [18] is a representative image-to-image translation network that utilizes U-Net as the generator and a patch-based fully convolutional network as the discriminator. Pix2pixHD [26] is a typical high-resolution photo-realistic image synthesis network, which is developed by using a coarse-to-fine generator and a multi-scale discriminator architecture. PAN [21] consists of two feed-forward convolutional networks (*e.g.*, a transformation network and a discriminative network) that capture more details and generate more realistic synthetic content. GFC [27] uses an auto-encoder as the generator with two adversarial loss

TABLE III
AVERAGE VALUES OF ASSESSMENT METRICS

Metric	PSNR↑	RMSE↓	SSIM↑	FSIM↑	Time (s)
Pix2pix [18]	21.487 ±0.409	0.079 ±0.007	0.758 ±0.010	0.837 ±0.019	11.225 ±0.293
Pix2pixHD [26]	22.368 ±0.291	0.073 ±0.005	0.827 ±0.015	0.846 ±0.016	12.420 ±0.299
PAN [21]	22.871 ±0.346	0.077 ±0.008	0.816 ±0.017	0.852 ±0.013	12.559 ±0.277
GFC [27]	22.639 ±0.338	0.075 ±0.007	0.814 ±0.009	0.862 ±0.014	14.621 ±0.258
Dental-GAN [19]	23.227 ±0.213	0.072 ±0.012	0.820 ±0.010	0.869 ±0.011	14.017 ±0.186
Stage-I GAN	22.797 ±0.278	0.071 ±0.009	0.751 ±0.011	0.841 ±0.015	11.463 ±0.217
Stage-I GroNet_OF	22.912 ±0.181	0.072 ±0.008	0.823 ±0.007	0.857 ±0.010	13.529 ±0.130
DCPR-GAN	23.304 ±0.168	0.068 ±0.008	0.845 ±0.005	0.887 ±0.007	14.210 ±0.107

Note: Values are denoted as mean ± standard deviation.

functions and the discriminator with a semantic regularization. Dental-GAN [19] is a full crown restoration network, which is developed by considering both the perceptual loss and groove loss measurements.

Using the original dental crown as the reference object, the reconstructed results are quantitatively evaluated using four objective evaluation metrics (*i.e.*, Peak Signal Noise Ratio (PSNR) [28], Root Mean Square Error (RMSE) [19], Structural Similarity Index Measure (SSIM) [29], Feature Similarity Index Measure (FSIM) [30]) are summarized in Table III. Pix2pix has lower values for PSNR, RMSE, SSIM, and FSIM, indicating that it cannot reconstruct more details of the occlusal surface. Compared with Pix2pix, the other seven methods provide better performance. DCPR-GAN achieves the best results overall for four quality indicators, validating the effectiveness of the proposed two-stage generative network and GroNet parser.

In addition, the running time for generating a dental crown of eight methods is provided. All of these networks have similar running complexity (about 11–15 seconds), but the DCPR-GAN method delivers the best reconstruction performance.

Furthermore, we also measured the root mean square (RMS) between the generated occlusal surface and the target crown, and performed a series of statistical analyses on the similarity measurements (see Fig. 9). First, a one-way ANOVA test was conducted to evaluate the similarity of the deviation measurements between the original and reconstructed images. For these eight methods, we found a statistically significant difference in deviation measurements ($p < 1e-8$). Similarly, using Kruskal-Wallis test, we found a statistically significant difference between DCPR-GAN and the other seven methods ($p \ll 1e-3$).

2) Qualitative Results: According to the distance-gray mapping relationship, the 3D mesh models of dental depth images are obtained using the mesh reconstruction method based on region growth. Fig. 10 provides three typical examples reconstructed by the above eight methods in which the occlusal fingerprints (olive-drab color) are extracted by a dental specialist. In addition, these

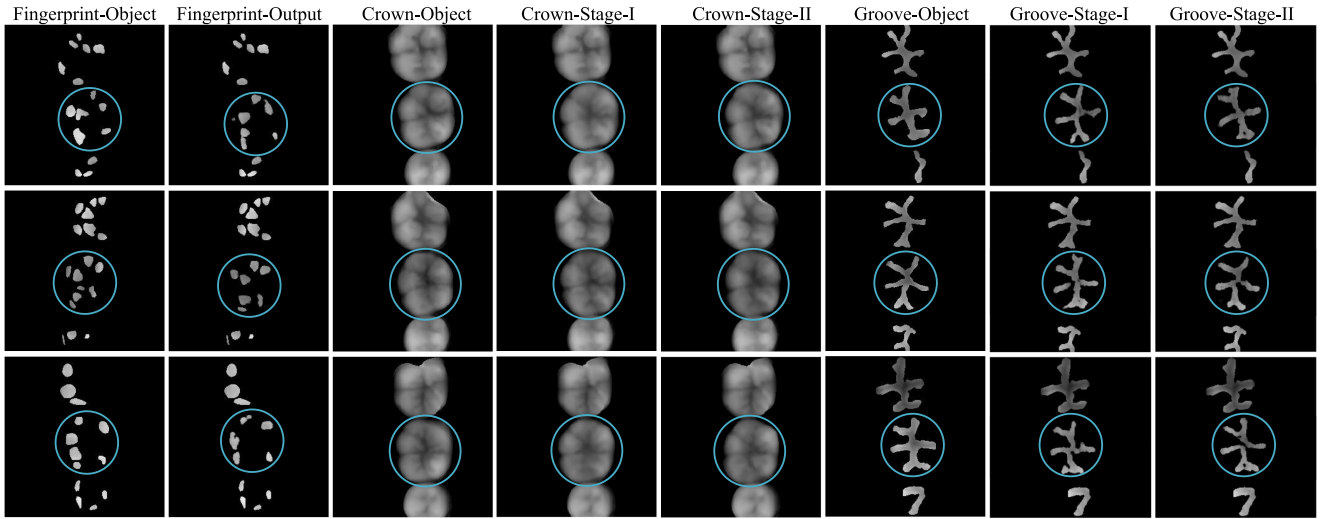


Fig. 8. Illustrations of the restoration results using the presented method. Aqua circle point out the generated details produced by our method.

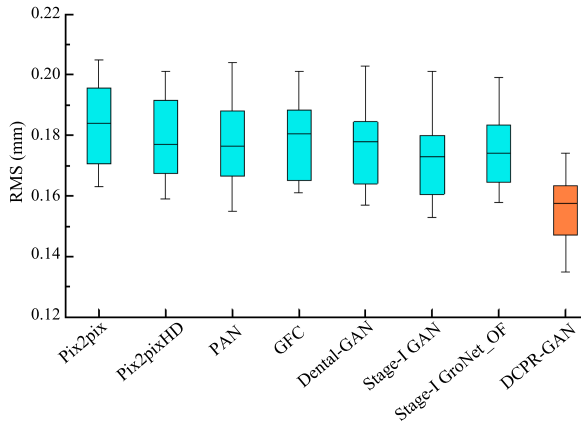


Fig. 9. Boxplots for deviation measurements.

three examples are selected from patients in different age groups and with different defective teeth (#36 or #46). The first column provides three preparation tooth samples (dark seagreen color), and the second column provides the corresponding ground-truth samples.

Fig. 10 indicates that the occlusal surfaces generated by Pix2pix, Pix2pixHD, and PAN have fewer occlusal finger- prints or a smoother occlusal groove. Meanwhile, GFC, Dental-GAN and Stage-I GAN provide better performance than Pix2pixHD and PAN. The distributions of the occlusal fingerprint and the occlusal groove generated by the Stage-I GroNet_OF are more reasonable than for the other methods. The results of DCPR-GAN are relatively close to the ground-truth samples, especially for the occlusal fingerprint distribution and the morphological characteristics of the occlusal surface. This further verifies the accuracy of the two-stage generation network.

To evaluate the quality of the occlusal surface, the deviation between the generated occlusal surface and the target crown is

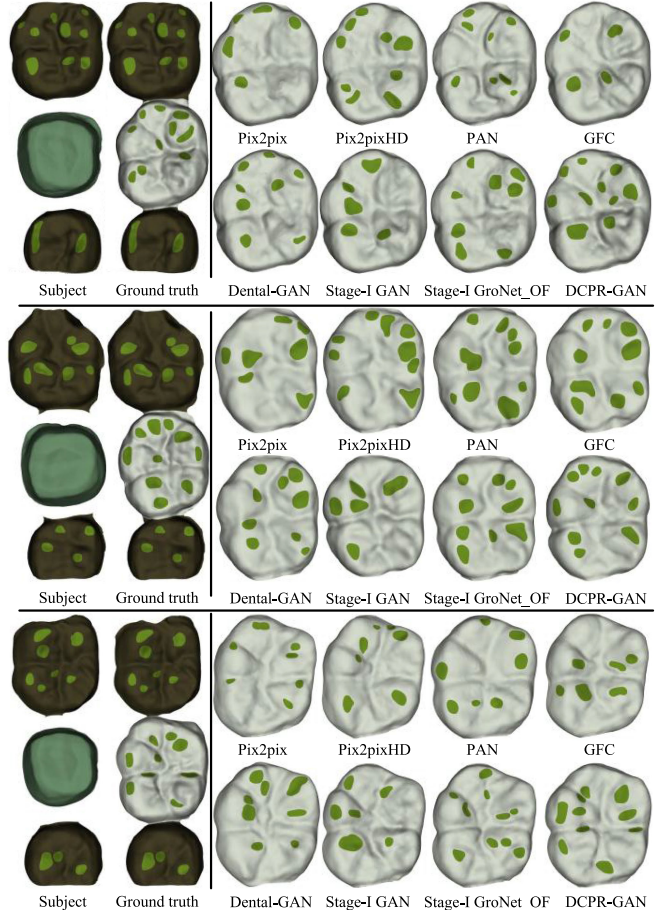


Fig. 10. Qualitative comparisons of three occlusal surface samples. The first column provides three typical dental samples with the dark seagreen color representing the defective region to be repaired, while the two adjacent teeth are in dark olivegreen color with the dark seagreen color representing the occlusal fingerprint. The second column provides the corresponding ground-truth samples, and the third to sixth columns provide the comparisons among the eight methods.

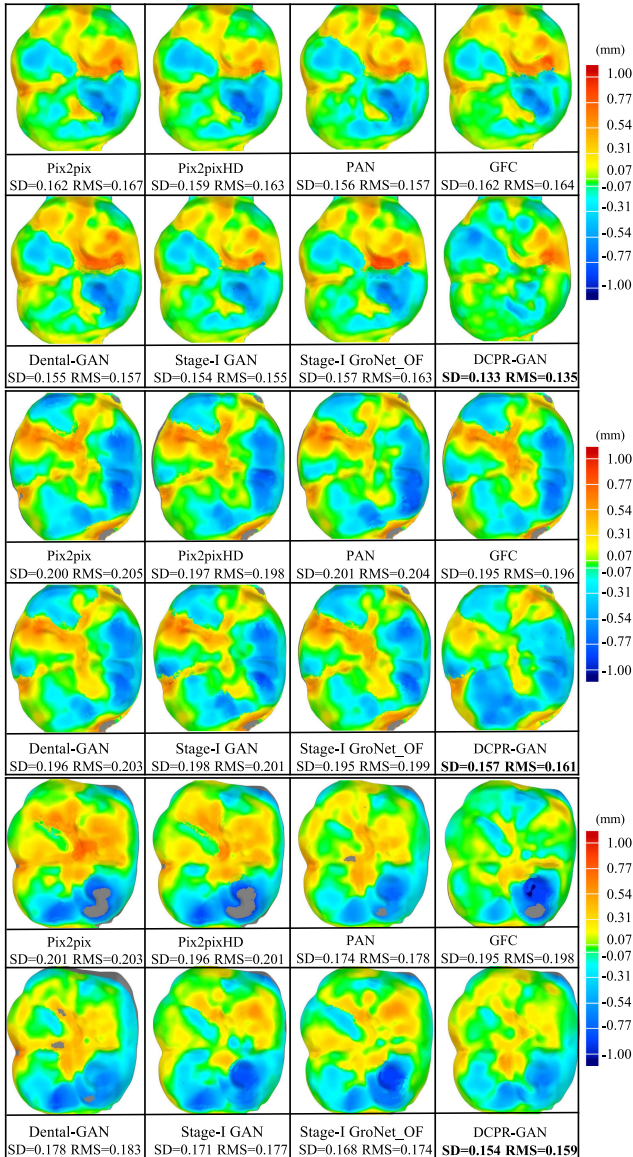


Fig. 11. Deviation analysis of the dental occlusal surface.

calculated under the constraint of the same proximal teeth. As shown in Fig. 11, the proposed DCPR-GAN method achieves much lower deviation values compared with the other seven methods. For instance, the standard deviation (SD) and root mean square (RMS) obtained by DCPR-GAN are 0.133 mm and 0.135 mm for the first example, which is lower than for the other seven methods by least 0.02 mm. Pix2pix achieves a relatively poor reconstruction performance. Compared with Pix2pix, Pix2pixHD and GFC yield better results, which can be attributed to the use of multi-scale discriminator architecture and a local-global discriminator network. In addition, since Stage-I GAN only uses the first-stage network of DCPR-GAN, its performance is much worse than DCPR-GAN for the occlusal surface reconstruction task. One possible reason is that Stage-I GAN only adds the spatial location constraint and the perceptual loss, whereas DCPR-GAN considers the additional impact of the functional characteristics of the occlusal surface.

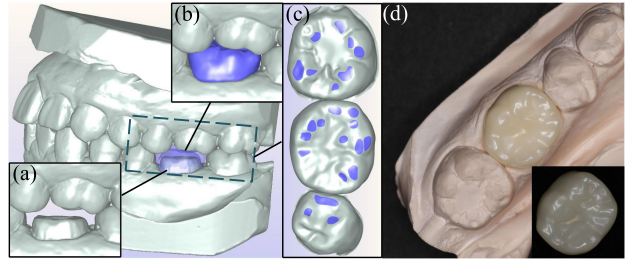


Fig. 12. Clinical example. (a) Preparation teeth and opposing teeth at the occluding positions, (b) Occlusion spatial relationship of the designed crown, (c) Occlusal fingerprint, (d) Wear result.

E. Realworld Dental Crown Prosthesis

One realworld dental crown prosthesis is chosen to demonstrate the clinical application of our proposed approach. A partially edentulous patient (original data #36) is presented including the proximal and opposing teeth at the occluding positions (Fig. 12(a)). The optimum parameters for DCPR-GAN model is trained to fit the generated occlusal surface to satisfy the correct masticatory function of the patient. The resulting occlusal surface image of the defective teeth is reconstructed into a 3D crown surface using the region growing method. Then, a dental crown with the functional occlusal surface is designed by combining the calculated adhesive layer and intermediate connector (Fig. 12(b)).

The occlusal fingerprint is mainly distributed in the buccal aspect of the mandibular molar (Fig. 12(c)) and is consistent with the results reported in the literature [23] and [31]. Moreover, the occlusal fingerprint with a similar shape reflects the comparable direction of movement and reproduces the natural occlusive movement. The outer surface has the personalized anatomical features of natural teeth and is basically harmonious with the proximal teeth (Fig. 12(d)).

IV. CONCLUSION AND DISCUSSION

In this article, we propose a new two-stage dental prosthesis restoration framework to automatically reconstruct the crown surface for a defective tooth. In the first stage, the global structure of the occlusal surface is captured to obtain an initial crown. In the second stage, the occlusal fingerprint constraint and the occlusal groove loss are added to yield the functional occlusal surface with crown-realistic details. This accurately creates a complete 3D dental crown prosthesis based on the designed intermediate connector. By evaluating DCPR-GAN based on a real database, the results show that DCPR-GAN outperforms the state-of-the-art methods.

Meanwhile, it should be noted that although DCPR-GAN method achieves the state-of-the-art performance in solving the challenging problem of functional occlusal surface generation, several technical issues should be considered in the future. 1) The examples here are developed only to investigate the teeth (#36 or #46) with the highest prevalence of caries. The reconstructed 3D model is based on the defective teeth from the generated depth images. Further exploration is needed to focus on other defective tooth categories. 2) The orthogonal projection method

is used to predict the depth information of the tooth data in the orthoscopic direction. For patients with irregular teeth, the tooth depth information can be incomplete. Therefore, multiple depth maps from different angles should be further considered to train a more robust network.

REFERENCES

- [1] E. D. Rekow, A. G. Erdman, D. R. Riley, and B. Klamecki, "CAD/CAM for dental restorations-some of the curious challenges," *IEEE Trans. Biomed. Eng.*, vol. 38, no. 4, pp. 314–318, Apr. 1991.
- [2] L. Liu, J. Xu, Y. Huan, Z. Zou, S.-C. Yeh, and L.-R. Zheng, "A smart dental health-IoT platform based on intelligent hardware, deep learning, and mobile terminal," *IEEE J. Biomed. Health Informat.*, vol. 24, no. 3, pp. 898–906, Mar. 2020.
- [3] Y. Pei *et al.*, "Personalized tooth shape estimation from radiograph and cast," *IEEE Trans. Biomed. Eng.*, vol. 59, no. 9, pp. 2400–2411, Sep. 2011.
- [4] F. J. Charlson *et al.*, "Global epidemiology and burden of schizophrenia: Findings from the global burden of disease study 2016," *Schizophrenia Bull.*, vol. 44, no. 6, pp. 1195–1203, 2018.
- [5] J. Wang *et al.*, "Augmented reality navigation with automatic marker-free image registration using 3-d image overlay for dental surgery," *IEEE Trans. Biomed. Eng.*, vol. 61, no. 4, pp. 1295–1304, Apr. 2014.
- [6] T. Vos *et al.*, "1990–2016: A systematic analysis for the global burden of disease study," *Lancet*, vol. 390, no. 10100, pp. 1211–1259, 2017.
- [7] Y. Tegawa and Y. Kinouchi, "Dental magnetic attachment: Toward third generation devices," *IEEE Trans. Biomed. Eng.*, vol. 55, no. 3, pp. 1185–1190, Mar. 2008.
- [8] X. Jiang *et al.*, "Robust tooth surface reconstruction by iterative deformation," *Comput. Biol. Med.*, vol. 68, pp. 90–100, 2016.
- [9] R. Sadid-Zadeh, A. Stylianou, and R. A. Wesson, "Prosthetic management of an existing transmandibular implant: A clinical report," *J. Prosthetic Dent.*, vol. 119, no. 5, pp. 693–697, 2018.
- [10] O. Kullmer, S. Benazzi, D. Schulz, P. Gunz, L. Kordos, and D. R. Begun, "Dental arch restoration using tooth macrowear patterns with application to Rudapithecus hungaricus, from the late Miocene of Rudabánya, Hungary," *J. Hum. Evol.*, vol. 64, no. 2, pp. 151–160, 2013.
- [11] M. Chung *et al.*, "Automatic registration between dental cone-beam CT and scanned surface via deep pose regression neural networks and clustered similarities," *IEEE Trans. Med. Imag.*, vol. 39, no. 12, pp. 3900–3909, Dec. 2020.
- [12] N. Torosdagli, D. K. Liberton, P. Verma, M. Sincan, J. S. Lee, and U. Bagci, "Deep geodesic learning for segmentation and anatomical landmarking," *IEEE Trans. Med. Imag.*, vol. 38, no. 4, pp. 919–931, Apr. 2018.
- [13] J. Zhang, Y. Gao, L. Wang, Z. Tang, J. J. Xia, and D. Shen, "Automatic craniomaxillofacial landmark digitization via segmentation-guided partially-joint regression forest model and multiscale statistical features," *IEEE Trans. Biomed. Eng.*, vol. 63, no. 9, pp. 1820–1829, Sep. 2016.
- [14] J. Hatvani, A. Horváth, J. Michetti, A. Basarab, D. Kouamé, and M. Gyöngy, "Deep learning-based super-resolution applied to dental computed tomography," *IEEE Trans. Radiat. Plasma Med. Sci.*, vol. 3, no. 2, pp. 120–128, Mar. 2018.
- [15] B. Zhang, N. Dai, S. Tian, F. Yuan, and Q. Yu, "The extraction method of tooth preparation margin line based on s-octree CNN," *Int. J. Numer. Methods Biomed. Eng.*, vol. 35, no. 10, 2019, Art. no. e3241.
- [16] C. Lian *et al.*, "Deep multi-scale mesh feature learning for automated labeling of raw dental surfaces from 3D intraoral scanners," *IEEE Trans. Med. Imag.*, vol. 39, no. 7, pp. 2440–2450, Jul. 2020.
- [17] J.-J. Hwang, S. Azernikov, A. A. Efros, and S. X. Yu, "Learning beyond human expertise with generative models for dental restorations," 2018, *arXiv:1804.00064*.
- [18] P. Isola, J.-Y. Zhu, T. Zhou, and A. A. Efros, "Image-to-image translation with conditional adversarial networks," in *Proc. IEEE Conf. Comput. Vis. Pattern Recognit.*, 2017, pp. 1125–1134.
- [19] F. Yuan *et al.*, "Personalized design technique for the dental occlusal surface based on conditional generative adversarial networks," *Int. J. Numer. Methods Biomed. Eng.*, vol. 36, no. 5, 2020, Art. no. e3321.
- [20] I. Goodfellow, Y. Bengio, A. Courville, and Y. Bengio, *Deep Learning*, vol. 1, Cambridge: MIT Press, 2016.
- [21] C. Wang, C. Xu, C. Wang, and D. Tao, "Perceptual adversarial networks for image-to-image transformation," *IEEE Trans. Image Process.*, vol. 27, no. 8, pp. 4066–4079, Aug. 2018.
- [22] S. Tian, N. Dai, X. Cheng, L. Li, Y. Sun, and H. Cui, "Relative trajectory-driven virtual dynamic occlusal adjustment for dental restorations," *Med. Biol. Eng. Comput.*, vol. 57, no. 1, pp. 59–70, 2019.
- [23] O. Kullmer, S. Benazzi, L. Fiorenza, D. Schulz, S. Bacso, and O. Winzen, "Occlusal fingerprint analysis: Quantification of tooth wear pattern," *Amer. J. Phys. Anthropol.*, vol. 139, no. 4, pp. 600–605, 2009.
- [24] C. Zhang, T. Liu, W. Liao, T. Yang, and L. Jiang, "Computer-aided design of dental inlay restoration based on dual-factor constrained deformation," *Adv. Eng. Softw.*, vol. 114, pp. 71–84, 2017.
- [25] M. Abadi *et al.*, "Tensorflow: Large-scale machine learning on heterogeneous distributed systems," 2016, *arXiv:1603.04467*.
- [26] T.-C. Wang, M.-Y. Liu, J.-Y. Zhu, A. Tao, J. Kautz, and B. Catanzaro, "High-resolution image synthesis and semantic manipulation with conditional gans," in *IEEE Conf. Comput. Vis. Pattern Recognit.*, 2018, pp. 8798–8807.
- [27] Y. Li, S. Liu, J. Yang, and M.-H. Yang, "Generative face completion," in *Proc. IEEE Conf. Comput. Vis. Pattern Recognit.*, 2017, pp. 3911–3919.
- [28] Z. Zhou, Y. Wang, Y. Guo, Y. Qi, and J. Yu, "Image quality improvement of hand-held ultrasound devices with a two-stage generative adversarial network," *IEEE Trans. Biomed. Eng.*, vol. 67, no. 1, pp. 298–311, Jan. 2019.
- [29] Y. Luo *et al.*, "Dehaze of cataractous retinal images using an unpaired generative adversarial network," *IEEE J. Biomed. Health Informat.*, vol. 24, no. 12, pp. 3374–3383, Dec. 2020.
- [30] L. Zhang, L. Zhang, X. Mou, and D. Zhang, "Fsim: A feature similarity index for image quality assessment," *IEEE Trans. Image Process.*, vol. 20, no. 8, pp. 2378–2386, Aug. 2011.
- [31] A. Vant Spijker, C. Kreulen, E. Bronkhorst, and N. Creugers, "Occlusal wear and occlusal condition in a convenience sample of young adults," *J. Dent.*, vol. 43, no. 1, pp. 72–77, 2015.